Journal of Catalysis 294 (2012) 128–135

Contents lists available at SciVerse ScienceDirect

Journal of Catalysis

journal homepage: www.elsevier.com/locate/jcat

Ir/Pt-HZSM5 for *n*-pentane isomerization: Effect of iridium loading on the properties and catalytic activity

H.D. Setiabudi [a], A.A. Jalil [a], S. Triwahyono [b,c,*]

[a] Institute of Hydrogen Economy, Faculty of Chemical Engineering, Universiti Teknologi Malaysia, 81310 UTM Johor Bahru, Johor, Malaysia
[b] Ibnu Sina Institute for Fundamental Science Studies, Faculty of Science, Universiti Teknologi Malaysia, 81310 UTM Johor Bahru, Johor, Malaysia
[c] Nanotechnology Research Alliance, Universiti Teknologi Malaysia, 81310 UTM Johor Bahru, Johor, Malaysia

ARTICLE INFO

Article history:
Received 26 May 2012
Revised 11 July 2012
Accepted 12 July 2012
Available online 11 August 2012

Keywords:
Ir/Pt-HZSM5
Protonic acid sites
Dimerization
Hydrogenolysis
n-Pentane isomerization

ABSTRACT

The effects of iridium loading on the properties of Ir/Pt-HZSM5 and *n*-pentane isomerization were studied. XRD, IR, and NMR results indicated that increasing iridium loading did not much change the properties of catalysts, but eliminated the perturbed silanol groups at 3700 and 3520 cm^{-1}, whereas IR and ESR spectroscopy confirmed that increasing iridium loading continuously decreased the permanent Lewis and Brønsted acid sites and inhibited the formation of protonic acid sites induced by hydrogen. At low iridium loading (0–0.3 wt%), cracking process proceed through dimerization-cracking step, whereas high iridium loading (0.5–2.0 wt%) reduces the contribution of dimerization-cracking step and promotes the contribution of hydrogenolysis. The excessive amount of iridium loading, with the presence of a low amount of active protonic acid sites and hydrogen gas, accelerated the hydrogenolysis process. The activity of Ir/Pt-HZSM5 was marginal in the absence of hydrogen, showing the dependence of activity on promotive effect of hydrogen.

1. Introduction

Bifunctional heterogeneous catalysts, consisting of a noble metal supported on microporous and mesoporous materials, have been widely studied because of their efficiency for the isomerization process and for the synthesis of high octane numbers [1–3]. It has been reported that the isomerization process over bifunctional heterogeneous catalysts was influenced by the hydrogen spillover phenomenon [4]. The promotive effect of hydrogen has been interpreted by the generation of protonic acid sites, in which the hydrogen migrates or spills over from noble metal sites onto the acidic oxide support, during the reaction. However, this hydrogen spillover effect has only been observed for a limited class of catalysts, including zeolite supported metal catalysts [1,5,6] and zirconia based acid catalysts [7–12], with different mechanisms and rate formation of protonic acid sites [13]. Therefore, the development of new catalysts with a better hydrogen spillover phenomenon and higher activity is necessary for the isomerization process.

In the recent years, the interest in bimetallic heterogeneous catalysts has been increasing, since the presence of a second metal can influence catalytic properties, improving their activity, stability, and selectivity. In particular, bimetallic catalysts composed by iridium and platinum were found to be active and stable for isomerization process. Yang and Woo [14] reported that bimetallic Pt–Ir/NaY maintained better activity for the *n*-heptane reforming reaction than the Pt/NaY catalyst, due to a decrease in the formation of coke. Additionally, Aboul-Gheit et al. [15] reported that the combination of platinum and iridium in the HZSM-5 zeolite produces a more active catalyst compared to the monometallic Pt/HZSM5 catalyst and thus enhanced the production of *iso*-hexane. Recently, we also have studied the effect of iridium on Pt-HZSM5 for the isomerization of *n*-pentane [6]. We found that the presence of 0.1 wt% iridium increased the number of strong Lewis acid sites and protonic acid sites via hydrogen spillover phenomenon and led to increase the selectivity of *iso*-pentane. In addition, the bonding of iridium oxide to perturbed silanol groups inhibited the formation of hydroxyl groups from molecular hydrogen at 3380, 3600 and 3680 cm^{-1}, where those hydroxyl groups may participate in the enhancement of the cracking reaction.

In the present report, the amount of iridium loaded on Pt-HZSM5 was studied, in order to elucidate the effects and limitations of iridium loading on the properties and activity of the Pt-HZSM5 catalyst. XRD, BET, and FTIR measurements were employed to observe the structural properties of the catalyst, and the adsorption of 2,6-lutidine was performed to identify the acidic nature of the catalyst. In addition, the hydrogen spillover phenomena of the catalysts were studied by hydrogen adsorption ESR and IR spectroscopy. In the catalytic activity studies, hydrogen and nitrogen were used as carrier gases in order to examine the promotive effect of hydrogen.

* Corresponding author. Fax: +60 7 5536080.
E-mail address: sugeng@utm.my (S. Triwahyono).

0021-9517/$ - see front matter © 2012 Elsevier Inc. All rights reserved.
http://dx.doi.org/10.1016/j.jcat.2012.07.012

2. Experimental

2.1. Catalyst preparation

Commercial HZSM5 (Zeolyst International) with Si/Al atomic ratio of 23 was used as a catalyst support. Pt-HZSM5 and Ir/Pt-HZSM5 were prepared according to the method described in previous report [6]. In brief, Pt-HZSM5 was prepared by incipient wetness impregnation of HZSM5 with the requisite quantity of $H_2PtCl_6{\cdot}H_2O$ (Merck) in aqueous solution to obtain 0.1 wt% Pt in the finished catalyst. After Pt impregnation, the product was dried at 383 K overnight and calcined at 823 K for 3 h in air. Subsequently, the prepared Pt-HZSM5 catalyst was impregnated with aqueous solution of $IrCl_3{\cdot}3H_2O$ (Merck) to obtained bimetallic Ir/Pt-HZSM5 catalyst, followed by drying at 383 K overnight and calcination at 823 K for 3 h in air. The content of iridium was adjusted to 0.1, 0.3, 0.5, 1.0, and 2.0 wt%. The prepared Ir/Pt-HZSM5 catalyst denoted as *x*Ir/Pt-HZSM5, where *x* is the weight percentage of iridium.

2.2. Catalyst characterization

The crystalline structure of the catalyst was determined by X-ray diffraction (XRD) recorded on a powder diffractometer (Bruker Advanced D8, 40 kV, 40 mA) using a Cu Kα radiation source in the range of $2\theta = 2–50°$. Percentage crystallinity was calculated using the average peak intensity at $2\theta = 7.9°$ and 8.9°, in which Pt-HZSM5 was used as a reference.

The BET analysis of the catalyst was determined by N_2 adsorption–desorption isotherm using a Quantachrome Autosorb-1 instrument. The catalyst was outgassed at 573 K for 3 h before being subjected to N_2 adsorption.

MAS NMR spectra were obtained using a Bruker Avance 400 MHz spectrometer. ^{29}Si MAS NMR spectra were recorded at a frequency of 79.4 MHz using a 4 μs radio frequency pulses, a recycle delay of 60 s and spinning rate of 7 kHz using a 4 mm zirconia sample rotor. ^{27}Al MAS NMR spectra were obtained at 104.2 MHz using pulse length of 1.9 μs, spin rate of 7 kHz, and relaxation time delay of 2 s.

Fourier Transform Infra Red (FTIR) measurements were carried out using Perkin–Elmer Spectrum GX FT-IR Spectrometer. The catalyst was prepared as a self-supported wafer and activated under hydrogen flow at 673 K for 3 h, followed by outgassing at 673 K for 3 h [10]. In the 2,6-lutidine adsorption process, the activated catalyst was exposed to 2 Torr of 2,6-lutidine at room temperature for 30 min, followed by outgassing at room temperature, 373 and 473 K for 30 min, respectively. The formation of protonic acid sites from molecular hydrogen was observed according to the method described in the literature [12]. The 2,6-lutidine pre-adsorbed catalyst was exposed to 100 Torr of hydrogen at room temperature. The catalyst was then heated stepwise from room temperature to 473 K in 50 K increments. All spectra were recorded at room temperature. In order to compare the surface coverage of the adsorbed species between different wafer thicknesses, all spectra were normalized using the overtone and combination vibrations of the MFI between 2100 and 1550 cm^{-1} after activation [16].

A JEOL JES-FA100 ESR Spectrometer was used to observe the formation of electron holes or unpaired electrons in vacuo heating and to observe the interaction of the electron holes or unpaired electrons with electrons formed from molecular hydrogen at room temperature to 473 K. The catalyst was outgassed at 673 K for 3 h followed by the introduction of 50 Torr of hydrogen at room temperature. The catalyst was then heated stepwise from room temperature to 473 K in 50 K increments [17,18].

2.3. Isomerization of n-pentane

The isomerization of *n*-pentane was performed in a microcatalytic pulse reactor according to the method described in the literatures [19]. Initially, 0.2 g of catalyst was treated in an oxygen stream (F_{Oxygen} = 100 ml/min) for 1 h followed by hydrogen stream ($F_{Hydrogen}$ = 100 ml/min) for 3 h at 673 K and cooled down to 548 K in a hydrogen stream. A dose of *n*-pentane (43 μmol) was passed over the activated catalyst, and the products were trapped at 77 K before flash-evaporation into an online 6090 N Agilent gas chromatograph equipped with HP-5 Capillary Column and FID detector. The intervals between each dose were kept constant at 20 min. Since all the catalysts reached steady state condition within 7 pulses (140 min), results at 7 pulses were used.

The conversion of *n*-pentane ($X_{n\text{-pentane}}$) was determined by

$$X_{n\text{-pentane}} = \frac{\sum A_i - A_{n\text{-pentane}}}{\sum A_i} \times 100 \quad (1)$$

where A_i and $A_{n\text{-pentane}}$ are corrected chromatographic area for particular compound and for residual *n*-pentane. The selectivity (S_i) and yield (Y_i) to particular product was calculated according to Eqs. (2) and (3), respectively.

$$S_i = \frac{A_i}{\sum A_i - A_{n\text{-pentane}}} \times 100 \quad (2)$$

$$Y_i = \frac{X_{n\text{-pentane}} \times S_i}{100} \quad (3)$$

3. Results and discussion

3.1. Structural properties of catalysts

Table 1 shows the XRD crystallinity and BET surface area of Pt-HZSM5 and Ir/Pt-HZSM5 catalysts with different iridium loading. Similar with our previous assignment [6], the introduction of 0.1 wt% iridium on Pt-HZSM5 slightly increased the percentage crystallinity of Pt-HZSM5 due to the elimination of the distorted aluminium sites caused by the interaction of iridium with perturbed silanol groups, which stabilizing the crystalline structure of Pt-HZSM5 and leading to a more ordered framework structure. An increase in the iridium content from 0.1 to 0.3 wt% did not alter the percentage crystallinity of the catalyst. However, further increases in the iridium content from 0.5 to 2.0 wt% resulted in a slight decrease in the percentage crystallinity, which may be due to the presence of excess amounts of iridium on the surface of Pt-HZSM5 or partially collapse of Pt-HZSM5 structure. Based on the XPS results in our previous assignment, the state of iridium on Pt-HZSM5 is Ir^{4+}, possibly as IrO_2 [6]. Thus, the excess amount of Ir species on the external surface of catalysts is most probably in the form of metal oxide (IrO_2). For BET surface area analysis, the presence of 0.1 wt% iridium in Pt-HZSM5 increased the BET surface area from 444 to 463 $m^2\ g^{-1}$ due to the increase (approximately 13.3%) in the crystallinity of Pt-HZSM5. However, the BET surface area of 0.1Ir/Pt-HZSM5 and 0.3Ir/Pt-HZSM5 catalysts are similar, indicating the 0.1–0.3 wt% iridium loading did not change the textural properties of the catalysts. Moreover, further increases in iridium loading, up to 2.0 wt%, led to a decrease in the BET surface area of the catalysts may be due to the blockage of a portion of the micropores with iridium oxide or partially collapse of Pt-HZSM5 structure. The change in the BET surface area of the catalyst, caused by the different amounts of iridium loading, was observed for an Ir/Beta catalyst, reported by Neaţu et al. [20]. They reported that increasing the amount of iridium loading (1.0–

Table 1
Structural properties of Pt-HZSM5 and iridium-modified Pt-HZSM5.

Catalysts	Iridium content (wt%)	XRD crystallinity (%)	BET surface area (m^2/g)
Pt-HZSM-5	0	100.0	444
0.1Ir/Pt-HZSM5	0.1	113.3	463
0.3Ir/Pt-HZSM5	0.3	113.5	460
0.5Ir/Pt-HZSM5	0.5	112.3	443
1.0Ir/Pt-HZSM5	1.0	102.6	419
2.0Ir/Pt-HZSM5	2.0	100.6	407

5.0 wt%) led to a decrease in the surface area of the Ir/Beta catalysts may be due to a blockage of the pores, caused by the deposition of iridium in large aggregates. A similar phenomenon was observed for a cobalt–iridium impregnated zirconium-doped mesoporous silica catalyst, in which the textural properties of the catalysts showed a moderate decrease as the iridium loading is increased, indicating the blockage of the mesopores with iridium species [21]. In contrast, Qun et al. [22] found that the specific surface area and total pore volume of all iridium-modified Fe-USY catalysts were similar, which indicated that the addition of iridium (0.1–2.0 wt%) into Fe-USY did not change the textural properties of Fe-USY, due to the well-controlled deposition of iridium onto Fe-USY.

^{27}Al and ^{29}Si MAS NMR offer a strong and effective tool for characterizing the structure of zeolite. In general, species with different structures or different environments will have a different chemical shift in their ^{27}Al and ^{29}Si MAS NMR spectra. Fig. 1A shows the ^{27}Al MAS NMR spectra of Pt-HZSM5 and Ir/Pt-HZSM5 catalysts with different iridium loading. Pt-HZSM5 catalyst shows three signals at 64, 55, and 0 ppm corresponding to the distorted tetrahedral sites, tetrahedral aluminium in the framework structure, and octahedrally coordinated extra-framework aluminium, respectively [23]. The introduction of iridium eliminated the peak at 64 ppm and slightly increased the intensity of the peak at 0 ppm. This result suggests that the presence of iridium could stabilize the MFI framework structure by eliminating the distorted aluminium sites in Pt-HZSM5, as previously observed [6]. As the iridium loading was increased from 0.1 to 2.0 wt%, there was no significant difference observed in the intensity of the signals at 55 and 0 ppm, indicating that increasing iridium loading (0.1–2.0 wt%) has little effect on the chemical environment of the aluminium atom.

The ^{29}Si MAS NMR spectra of Pt-HZSM5 and Ir/Pt-HZSM5 catalysts with different iridium loading are shown in Fig. 1B. For Pt-HZSM5, a dominant signal at approximately −112.8 ppm is assigned to $(\equiv SiO)_4Si$ while the shoulder signal between −103 and −108 ppm corresponded to $(\equiv SiO)_3Si$ in the HZSM5 framework [23]. Moreover, a small shoulder signal in the range of −120 to −135 ppm may be attributed to the cystallographically inequivalent sites in the Pt-HZSM5 catalyst [24]. The introduction of iridium on Pt-HZSM5 developed a new shoulder in the range between −90 and −103 ppm and eliminated the shoulder in the range between −120 and −135 ppm, indicating the formation of $(\equiv SiO)_2Si$ sites by eliminating the cystallographically inequivalent sites. As we previously observed [6], the elimination of the cystallographically inequivalent sites in Pt-HZSM5 may be related to the elimination of the distorted aluminium sites caused by the interaction of iridium with perturbed silanol groups of Pt-HZSM5. As the iridium loading was increased up to 2.0 wt%, no major changes were observed in the intensity of both signals, indicating that neither silicon nor aluminium strongly interacted with the iridium oxide. A similar trend was observed for molybdenum loaded on HMCM-22 zeolite reported by Ma et al. [25], in which no significant changes were observed in the ^{29}Si MAS NMR spectra of all Mo/HMCM-22 catalysts. All samples were prepared by impregnation of the HMCM-22 zeolite with an aqueous solution of ammonium heptamolybdate. Ma et al. suggested that the loading of molybdenum (2–10 wt%) does not destroy or change the silicate framework of the Mo/HMCM-22 catalysts.

Fig. 2 shows the IR spectra of the activated Pt-HZSM5 and iridium-modified Pt-HZSM5 catalysts in the region of hydroxyl groups. There were five bands observed in this region. The narrow band at 3740 cm^{-1} is assigned to the non-acidic terminal silanol groups (Si–OH) located on the external surface of the zeolite, while a shoulder band at approximately 3665 cm^{-1} is assigned to the extra-framework Al–OH species originating from limited hydrothermal degradation during the calcination process [26]. A band at 3610 cm^{-1} is assigned to the Brønsted OH band associated with bridging hydroxyl groups (Si(OH)Al) located inside the zeolite structure, whereas the weak band at 3700 cm^{-1} and broad band at 3520 cm^{-1} may be associated with the perturbation of OH groups through their surroundings by lattice defects or extra-lattice oxygen [27]. The introduction of iridium (0.1–2.0 wt%) on Pt-HZSM5 did not change the intensity of the bands at 3740, 3665 and 3610 cm^{-1}, indicating neither non-acidic terminal silanol groups, nor acidic bridging hydroxyl groups (Si(OH)Al) interacted with the iridium. However, the presence of 0.1 wt% iridium in Pt-HZSM5 broadened the band at 3740 cm^{-1} to higher wavenumber

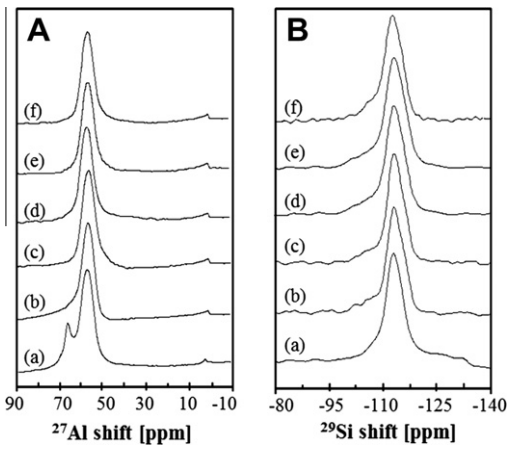

Fig. 1. (A) ^{27}Al MAS NMR (B) ^{29}Si MAS NMR spectra of (a) Pt-HZSM5; (b) 0.1Ir/Pt-HZSM5; (c) 0.3Ir/Pt-HZSM5; (d) 0.5Ir/Pt-HZSM5; (e) 1.0Ir/Pt-HZSM5; and (f) 2.0Ir/Pt-HZSM5.

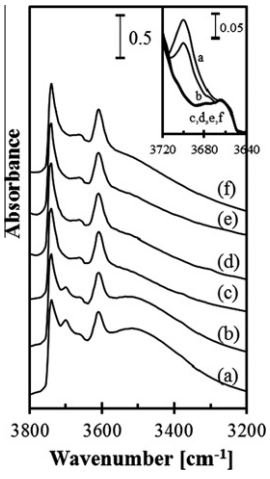

Fig. 2. IR spectra of activated (a) Pt-HZSM5; (b) 0.1Ir/Pt-HZSM5; (c) 0.3Ir/Pt-HZSM5; (d) 0.5Ir/Pt-HZSM5; (e) 1.0Ir/Pt-HZSM5; and (f) 2.0Ir/Pt-HZSM5 in the region of 3800–3200 cm^{-1}.

at 3745 cm^{-1} and slightly decreased the intensity of the bands at 3700 and 3520 cm^{-1}. As we previously reported [6], these results may be related to the formation of non-acidic geminal silanol groups at 3745 cm^{-1} by the interaction of iridium with perturbed silanol groups at 3700 and 3520 cm^{-1}. The formation of non-acidic geminal silanol groups at 3745 cm^{-1} is in agreement with the formation of $(\equiv SiO)_2Si$ in the NMR results. The interaction of iridium with perturbed silanol groups of Pt-HZSM5 most probably as $(\equiv SiO)_2Si(OH)_2(IrO_2)$. In contrast, as the iridium loading was increased up to 2.0 wt%, the bands corresponding to perturbed silanol groups at 3700 and 3520 cm^{-1} were eliminated after the addition of 0.3 wt% and no further changes were observed with increasing amount of iridium loading (0.5–2.0 wt%). The elimination of the bands at 3700 and 3520 cm^{-1} may be related to the interaction of iridium with perturbed silanol groups of Pt-HZSM5. This result indicated that all perturbed silanol groups of Pt-HZSM5 were possibly having a full interaction with iridium, when the amount of iridium loading achieved 0.3 wt%. The change of IR spectra with increasing metal loading was also observed in nickel loaded on a PtHY catalyst, as reported by Aziz et al. [17]. They reported that the addition of 0.1 wt% nickel eliminated the broad bands in the range of 3500–3720 cm^{-1} and partially decreased the band assigned to the terminal silanol groups at 3740 cm^{-1}. Additionally, as the nickel loading was increased up to 3.0 wt%, the intensity of the band corresponding to terminal silanol groups at 3740 cm^{-1} decreased markedly and a new band assigned to (–(OH)Ni), located on the surface of the zeolite framework, appeared at 3700 cm^{-1}.

3.2. Nature of acidity

The type of acid sites in all catalysts was qualitatively probed by 2,6-lutidine adsorption using IR spectroscopy. 2,6-lutidine (pK_b = 7.4), which demonstrated more basic character than the pyridine (pK_b = 8.8), is used to study the acidic nature of catalysts, particularly in the observation of the relatively weak Brønsted acid sites and the acidic centers of Lewis acid sites [28]. Fig. 3A shows the IR spectra of 2,6-lutidine adsorbed on activated Pt-HZSM5 and iridium-modified Pt-HZSM5 catalysts in the region of 1750–1350 cm^{-1}. The spectra were recorded after the adsorption of 2,6-lutidine at room temperature, followed by removal of 2,6-lutidine at 473 K. Since the catalysts were outgassed at 473 K, the acid sites under consideration are only strong acid sites that can retain 2,6-lutidine at the outgassing temperature of 473 K and below. All the catalysts showed the absorbance bands at 1700, 1680, 1650 and 1640 cm^{-1}, which are associated with the 2,6-lutidinium cations adsorbed on Brønsted acid sites. The absorbance bands at 1605, 1585, 1490, 1460, 1410, and 1385 cm^{-1} are assigned to the Lewis acid sites [29]. The changes in the acid sites are more clearly illustrated in Fig. 3B, in which the absorbance of the IR bands at Brønsted acid sites (1640 cm^{-1}) and Lewis acid sites (1585 cm^{-1}) were plotted as a function of iridium loading. The presence of 0.1 wt% iridium in Pt-HZSM5 slightly increased the intensity of the bands associated with the Brønsted and Lewis acid sites. Based on our previous assignment [6], the generation of acid sites may be due to the interaction of iridium with perturbed silanol groups, probably as $(\equiv SiO)_2Si(OH)_2(IrO_2)$. However, a slight decrease in the Brønsted and Lewis acid sites was observed with increasing iridium content from 0.1 to 2.0 wt%, which may be related to the presence of bulk iridium oxide on the external surface of the catalyst which may hinder the accessibility of acidic sites to the 2,6-lutidine probe molecule.

Partial coverage of the acid sites with iridium was also observed with the Ir/HZSM5 catalyst, as reported by Aboul-Gheit et al. [30]. The NH_3-TPD results showed that the addition of 0.35 wt% iridium to HZSM5 slightly decreased the values of ΔH from 98.4 to 87.5 J/g, indicating a small decrease in acid sites. The authors suggested that a slight decrease in the acid sites may be caused by the coverage of a portion of the acid sites with iridium. A similar phenomenon was observed with an Ir–Mo/HZSM5 catalyst in which the addition of 0.5 wt% iridium caused a decrease in all species of acid sites, from 553 K up to the end of the TPD run at 1073 K [31]. These authors also reported that a decrease in all species of acid sites was due to the coverage of a portion of the acid sites with iridium species.

3.3. Hydrogen molecule-originated protonic acid sites

Fig. 4A shows the changes in the IR spectra, when the 2,6-lutidine pre-adsorbed catalysts were heated in hydrogen at 473 K. As the catalysts were heated in hydrogen, the intensity of the bands at 1605, 1585, 1490, 1460, 1410 and 1385 cm^{-1}, corresponding to the Lewis acid sites, decreased with a concomitant increase in

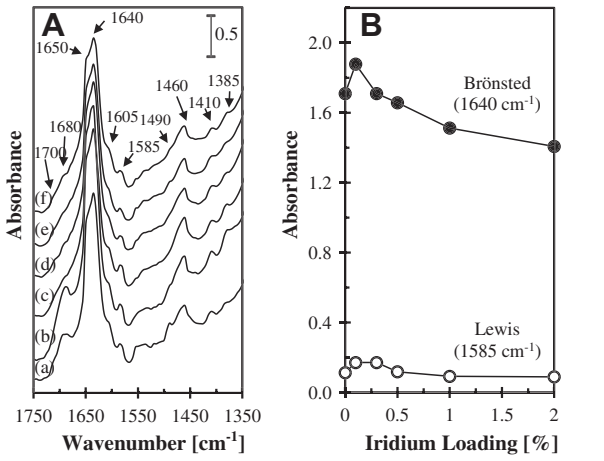

Fig. 3. (A) IR spectra of 2,6-lutidine adsorbed on activated (a) Pt-HZSM5; (b) 0.1Ir/Pt-HZSM5; (c) 0.3Ir/Pt-HZSM5; (d) 0.5Ir/Pt-HZSM5; (e) 1.0Ir/Pt-HZSM5; and (f) 2.0Ir/Pt-HZSM5 catalysts at room temperature followed by removal of 2,6-lutidine at 473 K. (B) Variations in the absorbance of the IR bands for Brønsted and Lewis acid sites after removal of 2,6-lutidine at 473 K.

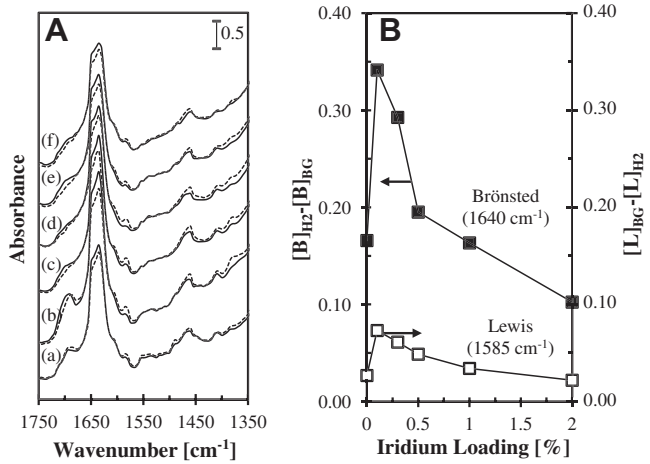

Fig. 4. (A) Spectral changes when 2,6-lutidine pre-adsorbed samples (dotted lines) were heated in the presence of hydrogen at 473 K (solid lines). (a) Pt-HZSM5;(b) 0.1Ir/Pt-HZSM5; (c) 0.3Ir/Pt-HZSM5; (d) 0.5Ir/Pt-HZSM5; (e) 1.0Ir/Pt-HZSM5; (f) 2.0Ir/Pt-HZSM5. (B) The changes in the peak intensity of the IR bands for Brønsted and Lewis acid sites when the catalysts were heated in hydrogen at 473 K. $[L_{1585}]_{BG}$ and $[B_{1640}]_{BG}$ represent the peak intensity of the Lewis and Brønsted acid sites before hydrogen adsorption. $[L_{1585}]_{H2}$ and $[B_{1640}]_{H2}$ represent the peak intensity of the Lewis and Brønsted acid sites in the presence of hydrogen at 473 K.

the intensity of the bands at 1700, 1680, 1650 and 1640 cm^{-1}, which are attributed to the peaks of 2,6-lutidine on Brønsted acid sites. This result demonstrates the formation of protonic acid sites, in the presence of hydrogen, with a simultaneous decrease in the number of Lewis acid sites, by switching the acidic character from Lewis acid sites to protonic acid sites. The effect of hydrogen was essentially similar for all catalysts, indicating that the concept of "molecular hydrogen-originated protonic acid sites" is applicable to Pt-HZSM5 and all Ir loaded on Pt-HZSM5 catalysts. It should be noted that the increase in the intensity of protonic acid sites is not similar to the decrease in the intensity of Lewis acid sites, because of the different extinction coefficients for the protonic and Lewis acid sites, as well as the ability of 2,6-lutidine to easily produce protonated species and its weaker affinity for Lewis acid sites.

The changes in the acid sites are more clearly illustrated in Fig. 4B, in which the absorbance of the IR bands at Brønsted acid sites (1640 cm^{-1}) and Lewis acid sites (1585 cm^{-1}) were plotted as a function of iridium loading. The introduction of 0.1 wt% iridium on Pt-HZSM5 slightly increased the formation of protonic acid sites originating from molecular hydrogen, whereas increasing amount of iridium loading (up to 2.0 wt%) slightly decreased the formation of protonic acid sites from molecular hydrogen. These results may be due to the changes in the number of strong Lewis acid sites, as evidenced by IR spectra of 2,6-lutidine adsorption. Although some differences were observed, the effect of hydrogen is essentially the same as that observed for Pt/HZSM5 [6], Zn/HZSM5 [5], Pt/MoO_3 [32], and MoO_3–ZrO_2 [12] catalysts. In contrast, no protonic acid sites were formed for a Ni/HY catalyst due to the inability of nickel to facilitate the formation of protonic acid sites from molecular hydrogen [17].

Fig. 5 shows the ESR signals of (A) 0.1Ir/Pt-HZSM5 and (B) 2.0Ir/Pt-HZSM5 catalysts, when the catalysts were outgassed at 673 K for 3 h, followed by heating in the presence of hydrogen at different temperatures. The ESR signal at $g = 1.99$ is assigned to the trapped electrons, or unpaired electrons, that have localized on metal cations (electron-deficient metal cations) [33]. As the catalysts were outgassed at 673 K for 3 h, the intensity of the ESR signal at $g = 1.99$ increased. This may be due to the desorption of hydroxyl groups from the surface of the catalysts, which subsequently leave the electron-deficient metal cations. The introduction of gaseous hydrogen, followed by heating, resulted in the formation of electrons and protonic acid sites where the electrons were trapped in the electron-deficient metal cations, resulting the reduction of the ESR signal at $g = 1.99$. Moreover, the protonic acid sites were stabilized near the surface oxygen atoms as hydrogen-bonded OH groups. Although both catalysts exhibited a similar phenomenon, 0.1Ir/Pt-HZSM5 showed largest changes in the intensity of the signal, over that of 2.0Ir/Pt-HZSM5, indicating that the formation of electrons via the hydrogen spillover mechanism is much easier for 0.1Ir/Pt-HZSM5, compared to that of 2.0Ir/Pt-HZSM5 catalyst.

The formation of electrons for Pt-HZSM5 and iridium-modified Pt-HZSM5 catalysts is more clearly illustrated in Fig. 6, in which the variation in the relative intensity of the ESR signal at $g = 1.99$ for all catalysts was plotted as a function of the heating temperature. As the heating temperature was increased, the variation in the relative intensity of the ESR signal at $g = 1.99$ decreased, due to the formation of electrons via the hydrogen spillover mechanism. Even though all catalysts exhibited a similar phenomenon, it is obvious that the generation of electrons is higher for 0.1Ir/Pt-HZSM5 catalysts, followed by 0.3, 0.5, 0, 1.0, and 2.0 wt%. The results of the ESR study are consistent with the FTIR study of hydrogen adsorption on 2,6-lutidine pre-adsorbed catalysts, in which the introduction of 0.1 wt% iridium increased the formation of protonic acid sites and electrons, whereas an increase in iridium loading decreased the formation of protonic acid sites and electrons.

The effect of hydrogen on the ESR signal is similar to the results observed for Pt/HY [17] and MoO_3–ZrO_2 [18] catalysts, in which heating the catalysts, in presence of hydrogen, partially eliminated the ESR signal assigned to the trapped electrons, or unpaired electrons, that have localized on metal cations (electron-deficient metal cations), representing the formation of electrons via hydrogen spillover phenomenon. However, for Ni/HY catalysts [17], heating the catalyst in the presence of hydrogen did not significantly change the ESR signal at $g = 1.9866$, indicating a low ability of the Ni/HY catalyst to form electrons via the hydrogen spillover phenomenon.

3.4. Isomerization of n-pentane

The catalytic activities of Pt-HZSM5 and Ir/Pt-HZSM5 catalysts with different amounts of iridium loading were evaluated with respect to *n*-pentane isomerization at 548 K in a microcatalytic pulse reactor, in which hydrogen or nitrogen was used as a carrier gas. The outlet consisted of cracking products, *iso*-pentane, residual *n*-pentane, and higher hydrocarbons. No cyclo-alkane product was observed, indicating that dehydrocyclization was not taking place on Ir/Pt-HZSM5. In fact, these types of catalysts are active in the ring-opening of cyclo-alkanes [34].

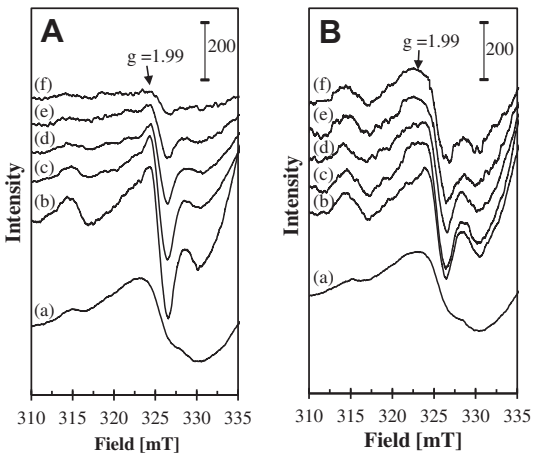

Fig. 5. ESR signals of (A) 0.1Ir/Pt-HZSM5 and (B) 2.0Ir/Pt-HZSM5. (a) Before outgassing; (b) after outgassing at 673 K and heated in the presence of 50 Torr hydrogen at (c) 323 K, (d) 373 K, (e) 423 K, and (f) 473 K.

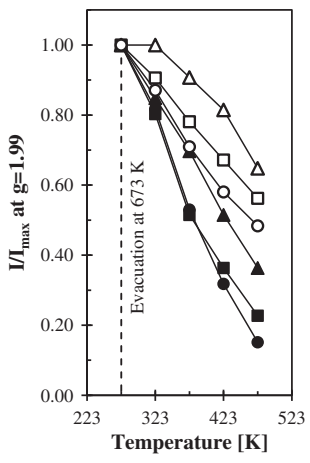

Fig. 6. Relative intensity of the ESR signal at $g = 1.99$ as a function of heating temperature. (○) Pt-HZSM5; (●) 0.1Ir/Pt-HZSM5; (■) 0.3Ir/Pt-HZSM5; (▲) 0.5Ir/Pt-HZSM5; (□) 1.0Ir/Pt-HZSM5; (Δ) 2.0Ir/Pt-HZSM5.

Fig. 7 shows the effect of iridium loading on the conversion of *n*-pentane, yield of *iso*-pentane and yield of cracking products in the presence of hydrogen or nitrogen. In the presence of nitrogen gas, all catalysts were not active in *n*-pentane isomerization. In fact, the yield of *iso*-pentane and cracking products did not typically exceed 5%, indicating that the presence of permanent strong Brønsted and Lewis acid sites do not directly affect the catalytic isomerization of *n*-pentane. This result also confirmed that thermal cracking does not take place on these catalysts. In the presence of hydrogen gas, the addition of 0.1 wt% iridium to Pt-HZSM5 has increased the yield of *iso*-pentane and decreased the yield of cracking products. As we previously observed [6], the enhancement in the yield of *iso*-pentane with the addition of 0.1 wt% iridium may be caused by the interaction of iridium with lattice defects or extra-lattice oxygen resulting in an increased in the number of strong Lewis and protonic acid sites from molecular hydrogen, whereas the suppression of cracking products may be caused by the inhibition of the formation of hydrogen bonding interactions from molecular hydrogen at 3680, 3600, and 3380 cm^{-1}. However, increasing iridium loading up to 0.3 wt% has reduced the conversion of *n*-pentane, while the ratio of *iso*- to cracking products was almost similar. The further loading of the iridium reduced continuously the yield of *iso*-pentane, but increased markedly the yield of cracking products. Additionally, the conversion of *n*-pentane and selectivity for cracking products exceeded than 98% on 2.0 wt% iridium loading on Pt-HZSM5.

The distribution of cracking products and higher hydrocarbons are shown in Fig. 8. At low iridium loading (0–0.3 wt%), cracking products consisted of methane, ethane, and propane. Additionally, small amount of *iso*-hexane and *n*-hexane were observed as higher hydrocarbons. However, only methane and ethane were observed for high iridium loading (0.5–2.0 wt%). The large amount of methane and ethane, without higher hydrocarbons, for high iridium loading indicates that the cracking process proceeds via a hydrogenolysis process, whereas the small amount of *iso*-hexane and *n*-hexane with the presence of cracking products (C_1–C_3) for low iridium loading (0–0.3 wt%) indicated the possibility of the dimerization-cracking route. The reduction in *iso*-pentane product followed by an increase in *n*-pentane conversion for 0.5–2.0 wt% iridium loading may be related to the increase in the perturbed silanol groups-covered by iridium, which lowered both Brønsted and Lewis acid sites. Lowering the acidity led to a reduction in the activity of isomerization and an excessive amount of iridium proceeded intensively the hydrogenolysis of *n*-pentane, in the presence of hydrogen, in the gas phase.

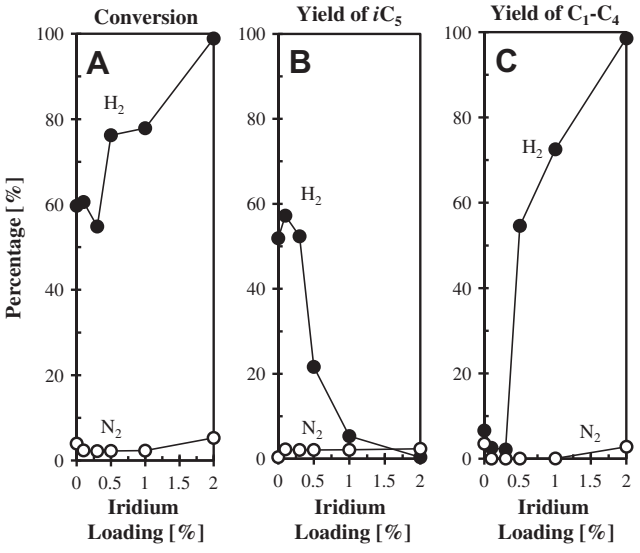

Fig. 7. Effect of Iridium loading on the (A) conversion of *n*-pentane, (B) yield of *iso*-pentane, and (C) yield of cracking products, in the presence of hydrogen (black symbol) and nitrogen (white symbol).

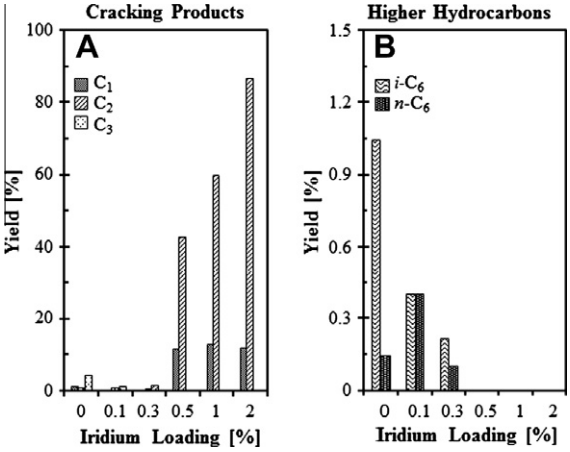

Fig. 8. Effect of Iridium loading on the distribution of (A) cracking products and (B) higher hydrocarbons in the presence of hydrogen.

Scheme 1 shows the plausible reaction mechanisms of *n*-pentane isomerization over Pt-HZSM5 and Ir/Pt-HZSM5 catalysts with different amounts of iridium loading. Isomerization process occurred for all amounts of iridium loading (0–2.0 wt%) while the cracking process route proceeds differently with amounts of iridium loading. Isomerization process proceeds by acid catalyzed reaction mechanism in which the isomerization was induced by the interaction between *n*-pentane and protonic acid site to form *n*-pentyl carbenium ion. Then, the carbenium ion was isomerized to mono- or multi-branched pentyl carbenium ion. The product of *iso*-pentane was produced by the interaction between branched pentyl carbenium ion and hydride ion followed by desorption form the surface of catalyst. The presence of protonic acid site and hydride ion was significant in *n*-pentane isomerization, and the formation of *iso*-pentane products increased by the concentration of protonic acid sites. At low iridium loading (0–0.3 wt%), cracking process proceeds via a dimerization-cracking reaction route in which the process was initiated with the dimerization of *n*-C_5 to form *n*-C_{10}, followed by the formation of cracking products and higher hydrocarbons. However, for higher iridium loading (0.5–2.0 wt%), the hydrogenolysis of *n*-pentane took place intensively and the possibility of a dimerization-cracking route can be excluded due to the absence of higher hydrocarbon products. Most probably, hydrogenolysis occurs on the surface of IrO_2 with hydrogen assisting in its gas phase and/or by contributing small amount of protonic acid sites.

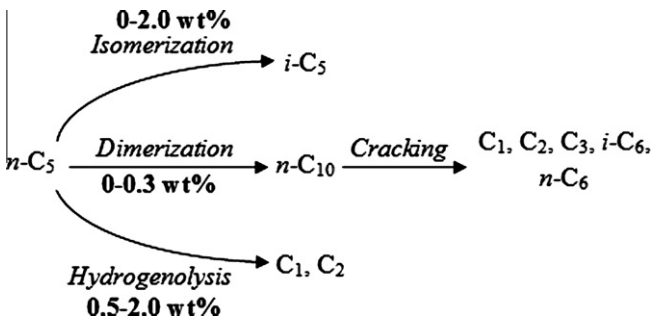

Scheme 1. Plausible reaction mechanisms for *n*-pentane isomerization over Pt-HZSM5 and Ir/Pt-HZSM5 catalysts with different amounts of iridium loading.

A similar phenomenon was observed for the conversion of heptane over Pt/H-Beta zeolite, as reported by Blomsma et al. [35]. Pt/H-Beta catalysts with different Pt loading (0.05–1.50 wt%) were prepared by incipient wetness impregnation. They found that low Pt loading (below 0.1 wt%) caused the cracking reaction to proceed via dimerization-cracking reaction. However, as Pt loading increased (up to 1.5 wt%), the hydrogenolysis route became dominant, due to the excessive amount of metal sites. In addition, it has been reported that the hydrogenolysis of *n*-alkanes usually takes place mainly on noble metals of Group VII [36–38] and their hydrogenolysis ability increase in the order of Pt < Pd < Ir < Rh < Ru [38]. Yang and Woo [14] studied the *n*-heptane reforming reaction over Pt–Ir/NaY catalyst in which Ir is present as agglomerated IrO_2 on the exterior surface while Pt is present as Pt^{2+} in the supercage and Pt^{4+} in sodalite cage after calcination of Pt–Ir/NaY at 500 °C. The catalytic activity study showed that an increase in the Ir content led to increase C_1–C_6 products due to the high activity of Ir for the hydrogenolysis reaction.

The promotive effects of hydrogen on hydrocarbon isomerization or cracking reactions have been reported by several research groups. Fujimoto et al. [1] studied the hydroconversion of *n*-pentane over hybrid catalysts under hydrogen and nitrogen atmospheres. In the absence of hydrogen, the conversion of *n*-pentane was dramatically reduced and an oligomerization reaction became dominant. They suggested that the spillover hydrogen play an important role in *n*-alkane hydroconversion. In addition, Shishido and Hattori [39] reported the promotive effect of hydrogen on the catalytic activity of Pt/SO_4^{2-}–ZrO_2 for cumene cracking reactions. They found that the presence of hydrogen enhanced the activity of Pt/SO_4^{2-}–ZrO_2 by forming the protonic acid sites generated from molecules of hydrogen. However, no promotive effect of hydrogen was observed on the SO_4^{2-}–ZrO_2 and Pt/ZrO_2 catalysts.

Fig. 9 shows the effect of iridium loading on the yield of *iso*-pentane, elimination of Lewis acid sites and the formation of protonic acid sites, induced by hydrogen in gas phase. The introduction of 0.1 wt% iridium to Pt-HZSM5 slightly increased the elimination of Lewis acid sites and increased the formation of protonic acid sites from molecular hydrogen. Additionally, 0.1 wt% iridium loading slightly increased the yield of *iso*-pentane from 51.89% to 57.22%. However, increasing iridium loading slightly decreased the elimination of Lewis acid sites and the formation of protonic acid sites and successively decreased the yield of *iso*-pentane. The inset figure shows the ratios of yield of *iso*-pentane to elimination of Lewis acid sites (Yield/ΔL) and to the formation of protonic acid sites (Yield/ΔB). The Yield/ΔL changes more extensively to that of Yield/ΔB, indicating that the yield of *iso*-pentane is directly correlated with the changes in the amount of formed Brønsted acid sites.

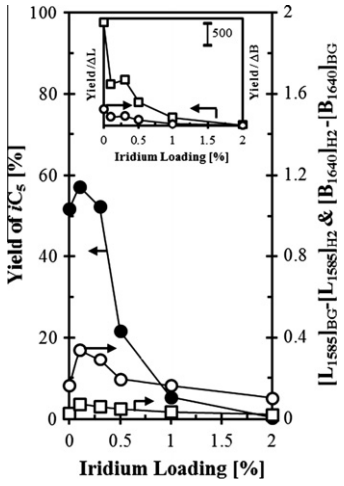

Fig. 9. Effect of Iridium loading on the formation of protonic acid sites and yield of *iso*-pentane. $[L_{1585}]_{BG}$ and $[B_{1640}]_{BG}$ represent the peak intensity of the Lewis and Brønsted acid sites before hydrogen adsorption. $[L_{1585}]_{H2}$ and $[B_{1640}]_{H2}$ represent the peak intensity of the Lewis and Brønsted acid sites in the presence of hydrogen at 473 K. (•) Yield of iC_5; (□) Lewis acid sites; (○) Brønsted acid sites.

4. Conclusion

Introduction of iridium (0.1–2.0 wt%) on Pt-HZSM5 did not interact with the non-acidic terminal silanol groups (3740 cm^{-1}), extraframework Al–OH species (3665 cm^{-1}) or acidic bridging hydroxyl groups (3610 cm^{-1}), but interacted with perturbed silanol groups of Pt-HZSM5 (3700 and 3520 cm^{-1}). This interaction eliminated the distorted tetrahedral sites caused by the presence of platinum. The presence of 0.1 wt% iridium slightly increased the number of Lewis and Brønsted acid sites and increased the number of protonic acid sites via hydrogen spillover phenomenon due to the interaction between iridium and perturbed silanol groups at 3700 and 3520 cm^{-1}. Moreover, the interaction between iridium and perturbed silanol groups resulted in the enhancement of *iso*-pentane selectivity.

However, an increase in iridium loading (0.3–2.0 wt%) did not significantly change the structural properties of catalysts, but decreased continuously the permanent Lewis and Brønsted acid sites and inhibited the changes of Lewis and Brønsted acid sites induced by hydrogen in the gaseous phase. In addition, the introduction of 0.3 wt% iridium totally eliminated the peaks corresponding to the perturbed silanol groups at 3700 and 3520 cm^{-1}. Further increases in iridium loading formed bulk iridium oxide on external surfaces. This led to increases in C_1 and C_2 products via hydrogenolysis of *n*-pentane. The presence of small number of higher hydrocarbon and C_1–C_3 cracking products for <0.3 wt% Ir loaded on Pt-HZSM5, indicated the possibility of the dimerization-cracking route. In particular, a large amount of protonic acid sites enhanced the isomerization of *n*-pentane, while a small amount of protonic acid sites, with the presence of hydrogen in gas phase on the surface of IrO_2, may enhance the hydrogenolysis of *n*-pentane. In general, the selectivity and yield of *iso*-pentane decreased with iridium loading, while the conversion of *n*-pentane increased, due to the increase in cracking products.

The catalytic activity studies confirmed that *n*-pentane isomerization over Ir/Pt-HZSM5 catalysts strongly depends on the promotive effect of hydrogen as a carrier gas. In fact, the yield of *iso*-pentane and cracking product did not typically exceed 5% for isomerization under nitrogen gas.

Acknowledgments

This work was supported by the Research University Grant, Universiti Teknologi Malaysia No. 00H95. Our gratitude also goes to Universiti Malaysia Pahang for the award of Skim Fellowship Universiti Malaysia (Herma Dina Setiabudi) and the Hitachi Scholarship Foundation for the Gas Chromatograph Instruments Grant.

References

[1] K. Fujimoto, K. Maeda, K. Aimoto, Appl. Catal. A: Gen. 91 (1992) 81.
[2] P. Cañizares, A. de Lucas, J.L. Valverde, F. Dorado, Ind. Eng. Chem. Res. 36 (1997) 4797.
[3] S. Triwahyono, A.A. Jalil, M. Musthofa, Appl. Catal. A: Gen. 372 (2010) 90.
[4] G.M. Pajonk, Appl. Catal. A: Gen. 202 (2000) 157.
[5] S. Triwahyono, A.A. Jalil, R.R. Mukti, M. Musthofa, N.A.M. Razali, M.A.A. Aziz, Appl. Catal. A: Gen. 407 (2011) 91.
[6] H.D. Setiabudi, A.A. Jalil, S. Triwahyono, N.H.N. Kamarudin, R.R. Mukti, Appl. Catal. A: Gen. 417–418 (2012) 190.
[7] K. Ebitani, J. Konishi, H. Hattori, J. Catal. 130 (1991) 257.
[8] T. Shishido, H. Hattori, Appl. Catal. A: Gen. 146 (1996) 157.

[9] S. Triwahyono, T. Yamada, H. Hattori, Catal. Lett. 85 (2003) 109.
[10] S. Triwahyono, Z. Abdullah, A.A. Jalil, J. Nat. Gas Chem. 15 (2006) 247.
[11] S. Triwahyono, T. Yamada, H. Hattori, Appl. Catal. A: Gen. 242 (2003) 101.
[12] N.N. Ruslan, N.A. Fadzlillah, A.H. Karim, A.A. Jalil, S. Triwahyono, Appl. Catal. A: Gen. 406 (2011) 102.
[13] W.C. Conner, J.L. Falconer, Chem. Rev. 95 (1995) 759.
[14] O.B. Yang, S.I. Woo, in: L. Guczi, F. Solymosi, P. Tetenyi (Eds.), New Frontiers in Catalysis, Proc. 10th Int. Cong. Catal., Budapest, Hungary,19–24 July 1992, Elsevier Science Publishers B.V., Amsterdam, 1993, p. 671.
[15] A.K. Aboul-Gheit, A.E. Awadallah, N.A.K. Aboul-Gheit, E.S.A. Solyman, M.A. Abdel-Aaty, Appl. Catal. A: Gen. 334 (2008) 304.
[16] A. Jentys, R.R. Mukti, H. Tanaka, J.A. Lercher, Micropor. Mesopor. Mater. 90 (2006) 284.
[17] M.A.A. Aziz, N.H.N. Kamarudin, H.D. Setiabudi, H. Hamdan, A.A. Jalil, S. Triwahyono, J. Nat. Gas Chem. 21 (2012) 29.
[18] N.N. Ruslan, S. Triwahyono, A.A. Jalil, S.N. Timmiati, N.H.R. Annuar, Appl. Catal. A: Gen. 413–414 (2012) 176.
[19] H.D. Setiabudi, S. Triwahyono, A.A. Jalil, N.H.N. Kamarudin, M.A.A. Aziz, J. Nat. Gas Chem. 20 (2011) 477.
[20] F. Neaţu, S. Coman, V.I. Pârvulescu, G. Poncelet, D.D. Vos, P. Jacobs, Top. Catal. 52 (2009) 1292.
[21] R. Moreno-Tost, E.R. Castellón, A. Jiménez-López, J. Mol. Catal. A: Chem. 248 (2006) 126.
[22] S. Qun, L. Landong, H. Zhengping, X.Z. Ping, Appl. Catal. B: Environ. 84 (2008) 734.
[23] G. Engelhardt, in: H. van Bekkum, E.M. Flanigen, P.A. Jacobs, J.C. Jansen (Eds.), Studies in Surface Science and Catalysis, vol. 137, Elsevier, Amsterdam, 2001, p. 387.
[24] W. Zhang, X. Bao, X. Guo, X. Wang, Catal. Lett. 60 (1999) 89.
[25] D. Ma, Y. Shu, X. Han, X. Liu, Y. Xu, X. Bao, J. Phys. Chem. B 105 (2001) 1786.
[26] J. Szanyi, M.T. Paffett, Micropor. Mater. 7 (1996) 201.
[27] J.A. Lercher, A. Jentys, in: J. Cejka, H. van Bekkun, A. Corma, F. Schuth (Eds.), Introduction to Zeolite Science and Practice, third ed., Elsevier, Amsterdam, 2007, p. 435.
[28] A. Corma, C. Rodellas, V. Fornes, J. Catal. 88 (1984) 374.
[29] C. Morterra, G. Cerrato, G. Meligrana, Langmuir 17 (2001) 7053.
[30] A.K. Aboul-Gheit, S.M. Aboul-Fotouh, N.A.K. Aboul-Gheit, Appl. Catal. A: Gen. 283 (2005) 157.
[31] A.K. Aboul-Gheit, A.E. Awadallah, S.M. El-Kossy, A.L.H. Mahmoud, J. Nat. Gas Chem. 17 (2008) 337.
[32] S. Triwahyono, A.A. Jalil, S.N. Timmiati, N.N. Ruslan, H. Hattori, Appl. Catal. A: Gen. 372 (2010) 103.
[33] I.R. Macdonald, R.F. Howe, X. Zhang, W. Zhou, J. Photochem. Photobiol. A: Chem. 216 (2010) 238.
[34] P.T. Do, W.E. Alvarez, D.E. Resasco, J. Catal. 238 (2006) 477.
[35] E. Blomsma, J.A. Martens, P.A. Jacobs, in: H. Chon, S.K. Ihm, Y.S. Uh (Eds.), Studies in Surface Science and Catalysis, vol. 105, Elsevier, Amsterdam, 1997, p. 909.
[36] S. Kuba, P. Lukinskas, R. Ahmad, F.C. Jentoft, R.K. Grasselli, B.C. Gates, H. Knözinger, J. Catal. 219 (2003) 376.
[37] J.L. Carter, J.A. Cusumano, J.H. Sinfelt, J. Catal. 20 (1971) 223.
[38] J.H. Sinfelt, D.J.C. Yates, J. Catal. 8 (1967) 82.
[39] T. Shishido, H. Hattori, J. Catal. 161 (1996) 194.